

Cite this: DOI: 10.1039/c3gc40547h

Flower-like mesoporous silica: a bifunctionalized catalyst for rhodium-catalyzed asymmetric transfer hydrogenation of aromatic ketones in aqueous medium†

Fei Gao, Ronghua Jin, Dacheng Zhang, Quanxi Liang, Qunqun Ye and Guohua Liu*

Functionalized flower-like mesoporous silica with a chiral organorhodium functionality incorporated within its silica framework is prepared through an assembly of chiral 4-((trimethoxysilyl)ethyl)phenylsulfonfyl-1,2-diphenylethylenediamine and tetraethoxysilane under a cooperative dual-template approach followed by complexation with organorhodium complexes. Structural characterization discloses its mesostructure and well-defined single-site chiral organorhodium functionality, while electron microscopy analyses reveal the uniformly distributed three-dimensional spherical flowers constructed by the stacking of leaf-shaped nanoflakes. In particular, as a bifunctionalized heterogeneous catalyst, it shows excellent catalytic activity and high enantioselectivity in the asymmetric transfer hydrogenation of aromatic ketones in aqueous medium (more than 99% conversion and up to 97% ee). The superior catalytic performance is attributed to the synergistic effect of the salient cetyltrimethylammonium bromide phase-transfer function and confined chiral organorhodium catalytic nature. Furthermore, this heterogeneous catalyst could be recovered easily and reused repeatedly (ten times) without affecting its ee value, showing a practical application in asymmetric synthesis.

Received 23rd March 2013,
Accepted 13th May 2013

DOI: 10.1039/c3gc40547h

www.rsc.org/greenchem

Introduction

Immobilization of homogeneous chiral organometallic catalysts onto mesoporous materials is a well-known method of solving the problem of expensive transition-metal recycling, while the green catalytic process is environmentally friendly. Recently, the exploration of organometallic-functionalized mesoporous silica materials for green asymmetric catalysis has attracted a great deal of interest.¹ The general features of easy separation, large specific surface area and pore volume are beneficial to enhance loadings and to improve the dispersibility of active species, resulting in a high catalytic performance. Furthermore, tunable pore dimensions and additional confinement effects can adjust the chiral microenvironment of the active center, presenting superior stereocontrol performance. In addition, the high thermal and mechanical stability in catalytic processes often leads to a high recycling efficiency, providing the opportunity for use in industrial applications. Although various silica-based mesoporous materials including

MCM-41,² SBA-15,³ SBA-16⁴ and PMO⁵ have been developed and some catalysts have exhibited high reactivity and enantioselectivity,^{2,4a,6} most of them still suffer from a low catalytic efficiency relative to their homogeneous counterparts. Accordingly, exploration of new silica-based supports and applications in environmentally friendly catalytic systems is still a challenge in asymmetric catalysis.

Three dimensional mesoporous silica with unique morphologies have a wide range of applications in drug delivery and bimolecular separations.⁷ In particular, functionalized flower-like mesoporous silica (FFMS), as a new type of silica-based support,⁸ shows significant advantages in asymmetric catalysis that have not yet been explored. Due to the special preparation strategy, the self-assembly of chiral functionalized materials often requires cetyltrimethylammonium bromide (CTAB) as a structure-directing template reagent, which inevitably leaves parts within the FFMS materials. This behavior can provide additional phase transfer function and may facilitate an asymmetric reaction in a two-phase catalysis system. More importantly, a unique mesoporous morphology with ultrathin aligned mesoporous nanoflakes has a relatively short nanochannel and special flower-like cavum that is beneficial for the accessibility/diffusion of substrates and improves the catalytic efficiency. In particular, the asymmetric transfer hydrogenation of ketones catalyzed by a *N*-sulfonylated

Key Laboratory of Resource Chemistry of Ministry of Education, Shanghai Normal University, Shanghai, 200234, China. E-mail: ghliu@shnu.edu.cn;

Fax: +86-21-64321819; Tel: +86-21-64321819

†Electronic supplementary information (ESI) available. See DOI: 10.1039/c3gc40547h

diamine-based organorhodium complex^{9,10} is a typical type of aqueous catalytic system. Taken together, it is reasonable to expect that the self-assembly of the chiral functionality within the FFMS and utilization of the additional phase transfer function of cetyltrimethylammonium bromide will contribute to high catalytic efficiency in an aqueous reaction system.

We are interested in mesoporous silica-supported chiral heterogeneous catalysts,¹¹ especially, in an effort to develop highly recyclable heterogeneous catalysts for cleaner and more benign chemical processes.¹² In this contribution, we develop a flower-like chiral TsDPEN-functionalized mesoporous silica *via* a cooperative dual-template approach and prepare a bifunctionalized heterogeneous catalyst, in which the residual CTAB functionality, as a phase transfer catalyst, and the chiral Cp*RhTsDPEN (Cp* = pentamethyl cyclopentadiene and TsDPEN = 4-methylphenylsulfonyl-1,2-diphenylethylenediamine) functionality, as a chiral promoter, are combined together within this material. As expected, this heterogeneous catalyst presents excellent catalytic efficiency in the asymmetric transfer hydrogenation of aromatic ketones in aqueous medium due to its bifunctional features, in which the CTAB functionality can greatly enhance the catalytic performance while the enantioselectivity can be maintained. Furthermore, the heterogeneous catalyst can be readily recycled and reused at least 10 times without reducing the catalytic efficiency. In particular, as a novel immobilized strategy, this research does not only open up a new route to immobilize homogeneous chiral catalysts, but also promotes the catalytic efficiency as a result of the synergistic effect of the salient phase-transfer function and the confined chiral organorhodium nature.

Experimental

General

All experiments, which were sensitive to moisture or air, were carried out under an Ar atmosphere using standard Schlenk techniques. 2-(4-Chlorosulfonylphenyl)ethyltrimethoxysilane, 4-(methylphenylsulfonyl)-1,2-diphenylethylenediamine [(*S,S*)-TsDPEN], the surfactant cetyltrimethylammonium bromide (CTAB), tetraethoxysilane (TEOS) and [Cp*RhCl₂]₂ were purchased from Sigma-Aldrich Company Ltd. and used as received. Compound [(*S,S*)-DPEN-SO₂Ph(CH₂)₂Si(OMe)₃] and the pure material was synthesized according to the reported literature.^{12b}

Catalyst preparation

Preparation of TsDPEN-functionalized-FFMS (2). A typical procedure was as follows: 0.20 g of CTAB was dissolved in 96.0 g of deionized water under stirring at room temperature. Then 0.10 g of CaO (mol ratio of Ca/Si = 0.3) was added into the solution, the resulting mixture was ultrasonically irradiated for 1 h under ambient conditions with a ultrasonic cleaning instrument (KUDOS, SK3300H, 59 kHz) immersed directly in the solution (the power used was 160 W). The solution was raised to 353 K. Then, TsDPEN-derived silica (**1**) (0.25 g,

0.50 mmol) was added and underwent hydrolytic decomposition for 1 min, then tetraethoxysilane (TOES) (1.08 g, 5.2 mmol) was rapidly added *via* injection (pH = 11.8). After stirring for an additional 2 h, the reaction mixture was transferred into a Teflon-lined autoclave and aged at 383 K under static conditions for 72 h. The surfactant was extracted by refluxing with a HCl-ethanol solution for 8 h. The resulting products were collected by filtration and dried at 333 K *in vacuum* overnight to afford **2** (0.65 g) as a white powder. IR (KBr) cm⁻¹ (s: strong peak, m: medium peak and w: weak peak): 3427.2 (s), 2978.4 (w), 2926.6 (w), 1625.6 (m), 1495.9 (w), 1459.5 (w), 1402.3 (w), 1384.1 (w), 1078.8 (s), 949.6 (s), 800.6 (s), 700.8 (s), 668.6 (s) 575.4 (w), 462.5 (s). Elemental analysis (%): C 12.01, H 1.73, N 1.01, S 0.71. *S*_{BET}: 486.67 m² g⁻¹, *V*_{pore}: 0.34 cm³ g⁻¹, *d*_{pore}: 5.34 nm. ²⁹Si MAS NMR (300 MHz): T² (δ = -59.1 ppm), T³ (δ = -69.2 ppm), Q² (δ = -92.9 ppm), Q³ (δ = -102.0 ppm), Q⁴ (δ = -110.0 ppm). ¹³C CP MAS NMR (161.9 MHz): 136.2 (Ar-C), 128.0 (Ar-C), 76.3 (NH-CH-Ph), 60.2 (OCH₃ and OCH₂CH₃), 36.9 (CH₂-Ar), 29.2 (OCH₂CH₃), 17.9 (CH₂-Si) ppm.

Preparation of the heterogeneous catalyst 3. In a typical synthesis, to a stirred suspension of **2** (1.0 g) and NEt₃ (1.00 mL, 16.5 mmol) in 20 mL dry CH₂Cl₂ was added [Cp*RhCl₂]₂ (82.0 mg, 0.15 mmol) at room temperature. The resulting mixture was stirred at room temperature for 12 h. The mixture was then filtered through filter paper and rinsed with excess CH₂Cl₂. After Soxhlet extraction in CH₂Cl₂ solvent to remove homogeneous and unreacted start materials for 24 h, the solid was dried at 333 K *in vacuum* for 12 h to afford the catalyst **3** (1.06 g, 73.2% relative to **2**) as an orange powder. ICP analysis shows that the Rh loading-amount was 27.18 mg (0.26 mmol) per gram catalyst. IR (KBr) cm⁻¹: 3426.9 (s), 2978.4 (w), 2926.6 (w), 1625.1 (m), 1495.9 (w), 1459.5 (w), 1402.3 (w), 1384.1 (w), 1078.8 (s), 948.6 (s), 769.6 (s), 700.8 (s), 569.4 (w), 459.5 (s). Elemental analysis (%): C 13.99, H 2.06, N 0.95, S 0.66. *S*_{BET}: 232.45 m² g⁻¹, *V*_{pore}: 0.19 cm³ g⁻¹, *d*_{pore}: 4.25 nm. ²⁹Si MAS NMR (300 MHz): T³ (δ = -68.7 ppm), Q² (δ = -93.1 ppm), Q³ (δ = -102.0 ppm), Q⁴ (δ = -110.3 ppm). ¹³C CP MAS NMR (161.9 MHz): 136.2 (Ar-C), 127.9 (Ar-C), 94.4 (Cp*-C), 76.3 (NH-CH-Ph), 61.1 (OCH₃), 36.9 (CH₂-Ar), 29.2 (OCH₂CH₃), 17.5 (CH₂-Si), 9.3 (CpCH₃) ppm.

Characterization

The amount of Rh loaded in the catalyst was analyzed using an inductively coupled plasma optical emission spectrometer (ICP, Varian VISTA-MPX). Fourier transform infrared (FT-IR) spectra were collected on a Nicolet Magna 550 spectrometer using KBr method. X-Ray powder diffraction (XRD) was carried out on a Rigaku D/Max-RB diffractometer with Cu-Kα radiation. Scanning electron microscopy (SEM) images were obtained using a JEOL JSM-6380LV microscope operating at 20 kV. Transmission electron microscopy (TEM) images were performed on a JEOL JEM2010 electron microscope at an acceleration voltage of 220 kV. X-Ray photoelectron spectroscopy (XPS) measurements were performed on a Perkin-Elmer PHI 5000C ESCA system. All the binding energies were

calibrated using the contaminant carbon ($C_{1s} = 284.6$ eV) as a reference. Thermal gravimetric analysis (TGA) was performed with a Perkin-Elmer Pyris Diamond TG analyzer under an air atmosphere with a heating ramp of 5 K min^{-1} . Solid-state ^{13}C (100.5 MHz) and ^{29}Si (79.4 MHz) CP MAS NMR were obtained on a Bruker DRX-400 spectrometer.

General procedure for the asymmetric transfer hydrogenation of aromatic ketones

A typical procedure was as follows: the heterogeneous catalyst **3** (7.58 mg, 2.00 μmol of Rh based on ICP analysis), HCO_2Na (0.68 g, 10.0 mmol), ketone (0.20 mmol) and 2.0 mL water were added to a 10 mL round bottom flask in turn. The mixture was allowed to react at 313 K for 0.5–5 h. During that time, the reaction was monitored constantly by TLC. After completion of the reaction, the heterogeneous catalyst was separated *via* centrifuge ($10\,000\text{ r min}^{-1}$) for the recycling experiment. The aqueous solution was extracted by Et_2O ($3 \times 3.0\text{ mL}$). The combined Et_2O was washed with brine twice and dehydrated with Na_2SO_4 . After the evaporation of Et_2O , the residue was purified by silica gel flash column chromatography to afford the desired product. The conversion and the ee value could be determined by chiral GC using a Supelco β -Dex 120 chiral column ($30\text{ m} \times 0.25\text{ mm}$ (i.d.), $0.25\text{ }\mu\text{m}$ film) or a HPLC analysis with a UV-Vis detector using a Daicel OD-H chiralcel column ($\Phi\ 0.46 \times 25\text{ cm}$).

Results and discussion

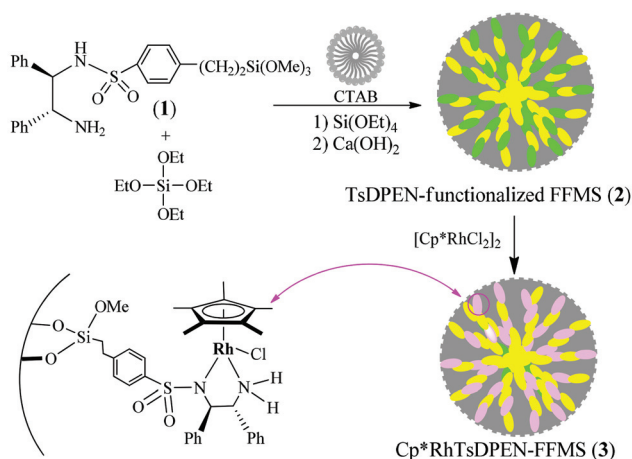
Synthesis and structural characterization of the heterogeneous catalyst

The flower-like organorhodium-functionalized mesoporous silica, abbreviated as $\text{Cp}^*\text{RhTsDPEN-FFMS}$ (**3**), was prepared *via* an assembly strategy followed by an *in situ* complexation approach as outlined in Scheme 1. Firstly, the TsDPEN-derived silica (**1**) was synthesized according to our previous report.^{11b} The assembly of tetraethoxysilane (TOES) and TsDPEN-derived

silane (**1**) using the cooperative dual-template reagents of an inorganic layered calcium silicate hydrates template and a liquid crystal template⁸ gave TsDPEN-functionalized-FFMS (**2**) in the form of a white powder. Finally, the direct complexation of **2** with $(\text{Cp}^*\text{RhCl}_2)_2$ followed by trimming of the nanopore *via* thorough Soxhlet extraction afforded the catalyst **3** in the form of an orange powder (see ESI in Fig. S1†). The inductively coupled plasma (ICP) optical emission spectrometer analysis showed that the Rh loading was 21.18 mg (0.21 mmol) per gram catalyst while the elemental analysis disclosed that the amount of S was 0.21 mmol per gram of catalyst, calculated from the mass % of S atoms (S 0.66%), in which the 1 : 1 mole ratio of Rh to S atoms suggested the generation of a single-site $\text{Cp}^*\text{RhTsDPEN}$ functionality within the FFMS silicate network.

The incorporation of the $\text{Cp}^*\text{RhTsDPEN}$ functionality in the silicate network could be further confirmed by the solid-state ^{13}C cross polarization (CP) MAS NMR spectra. As shown in Fig. 1, besides the general peaks of the chiral TsDPEN ligand, it was easily found that the catalyst **3** displayed clear characteristic peaks around 94 ppm corresponding to the C atoms of the Cp rings, and the peaks around 9 ppm corresponded to the C atoms of the methyl groups connected to the Cp rings, in which all these peaks were strongly similar to those of its homogeneous counterpart $\text{Cp}^*\text{RhTsDPEN}$,¹³ confirming that the catalyst **3** possessed the same well-defined single-site active center as its homogeneous counterpart. It is worth mentioning that the peaks around 14 and 30 ppm correspond to the C of the methyl (or methylene) groups without connection to a nitrogen atom in the CTAB molecule, and the peaks around 60 ppm correspond to the C atoms of the methyl (or methylene) groups connected to nitrogen atoms in the CTAB molecule; in which these peaks, the parts of the peaks in the TsDPEN moiety and the peak of the nonhydrolyzed methoxide groups ($\text{CH}_3\text{O-}$)¹⁴ were overlapped together as marked in Fig. 1. In addition, other peaks denoted by asterisks were the rotational sidebands that often appear in the CP MAS high speed rotation process.¹⁵

In addition, the ^{29}Si magic angle spinning (MAS) NMR spectra of the catalyst **3** revealed two groups of typical signals



Scheme 1 Synthesis of the heterogeneous catalyst **3**.

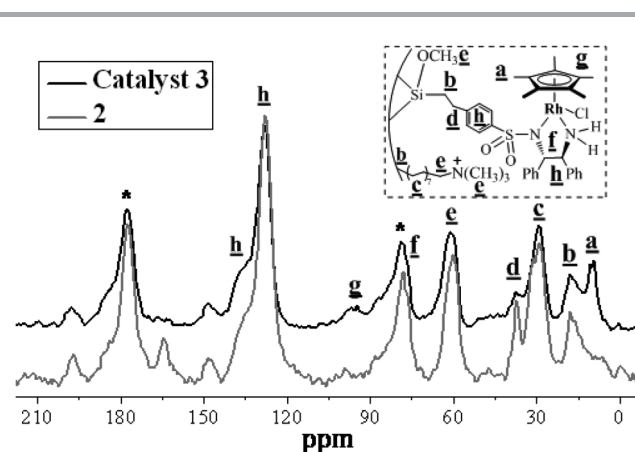


Fig. 1 The ^{13}C CP MAS NMR spectra of **2–3**.

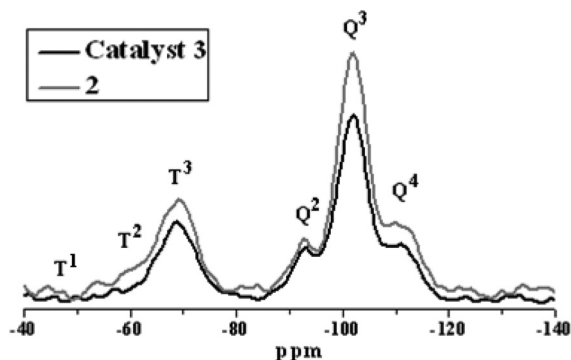


Fig. 2 The ^{29}Si CP MAS NMR spectrum of 2–3.

(Q and T signals) distributed broadly from -50 to -150 ppm, as marked in Fig. 2, in which the up-field Q signals originate from the inorganic molecules of the TEOS functionality while the downfield T signals are derived from the organic molecules of the silylether groups. Typical isomer shift values were $-91.5/-101.5/-110$ ppm for the $Q^2/Q^3/Q^4$ signals $\{[(\text{HO})_2\text{Si}(\text{OSi})_2]/[(\text{HO})\text{Si}(\text{OSi})_3]/[\text{Si}(\text{OSi})_4]\}$ and are $-48.5/-58.5/-67.5$ ppm for the $T^1/T^2/T^3$ signals $\{[\text{R}(\text{HO})_2\text{SiOSi}]/[\text{R}(\text{HO})\text{Si}(\text{OSi})_2]/[\text{RSi}(\text{OSi})_3]\}$.¹⁶ As compared with these typical signals, the strongest Q^3 peak in the Q series suggested that the catalyst 3 possessed a mainly inorganosilicate framework of $(\text{HO})\text{Si}(\text{OSi})_3$, while the strongest T^3 peak in the T series indicated that the organosilicate $[\text{RSi}(\text{OSi})_3]$ ($\text{R} = \text{Cp}^*\text{RhTsDPEN}$ functionality) was the main part of the silica wall in its FFMS silicate network.¹⁷

Fig. 3 shows the TG/DTA curves of the catalyst 3 treated in air. It was found that an endothermic peak around 355 K, with weight loss of 10.2%, could be attributed to the release of physically adsorbed water. Furthermore, two exothermic peaks around 636 K and 701 K with a total weight loss of 23.3% could be assigned to the oxidation of the organic moieties (including $\text{Cp}^*\text{RhTsDPEN}$ functionalities and the residual CTAB surfactants¹⁸). When eliminating the contribution of water, the total weight loss of organic moieties was 25.9%. In sharp contrast to the TG/DTA curve of the pure FMS material, with a 9.6% weight loss for the residual CTAB¹⁸ (see ESI in

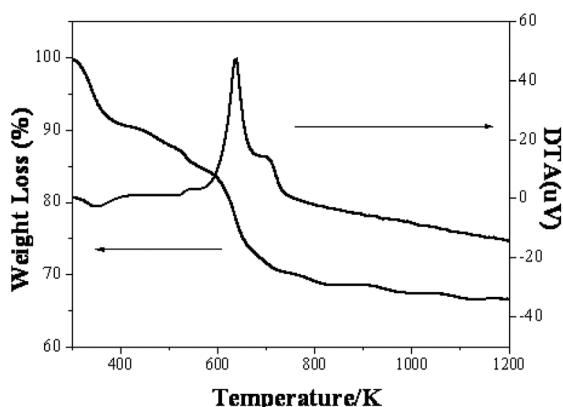


Fig. 3 The TG/DTA curves of catalyst 3.

Fig. S2†), it was found that 16.3% of the $\text{Cp}^*\text{RhTsDPEN}$ functionality was loaded within its FFMS silicate network, which was nearly consistent with 27.18 mg (0.26 mmol) of the Rh loading per gram catalyst detected by ICP analysis.

In order to investigate the electronic state of the rhodium center, the X-ray photoelectron spectroscopy (XPS) of the catalyst 3 and its homogeneous counterpart were investigated. As shown in Fig. 4, the XPS spectra of the catalyst 3 gave a Rh $3d_{5/2}$ binding energy of around 309.43 eV, indicating that the rhodium center was in the trivalent state.¹⁹ More importantly, it was found that catalyst 3 had almost the same Rh $3d_{5/2}$ electron binding energy as the parent $\text{Cp}^*\text{RhTsDPEN}$ (309.43 eV versus 309.38 eV), suggesting that the rhodium center within the FFMS silicate network retained its original chiral coordination microenvironment.

The mesostructure and morphology of catalyst 3 were further characterized using a nitrogen adsorption–desorption technique, along with scanning electron microscopy (SEM) and transmission electron microscopy (TEM). As shown in Fig. 5, the nitrogen adsorption–desorption isotherm revealed that catalyst 3 was mesoporous due to the typical type IV

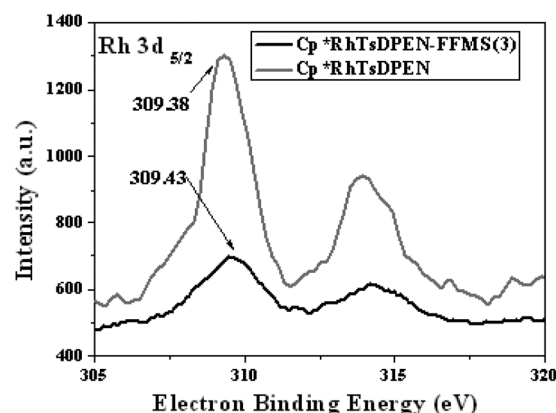


Fig. 4 The XPS spectra of $\text{Cp}^*\text{RhTsDPEN}$ and 3.

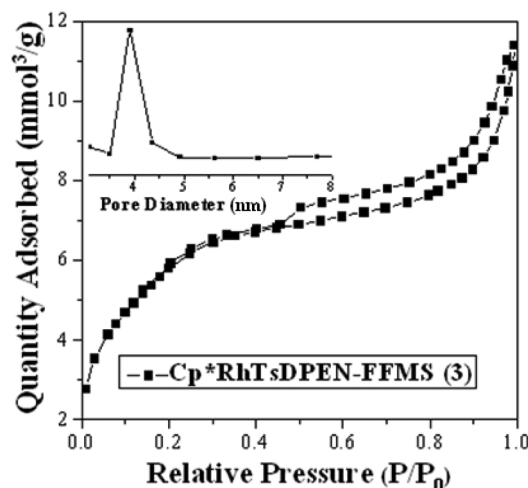


Fig. 5 The nitrogen adsorption–desorption isotherm of the catalyst 3.

isotherms with a H_1 hysteresis loop and a visible step at $P/P_0 = 0.40$ – 1.0 , which could be further confirmed by the powder X-ray diffraction (see ESI in Fig. S3†). Furthermore, the SEM image (Fig. 6a) clearly shows that catalyst **3** was composed of uniformly distributed spherical flowers with a particle size of about 750 nm, in which a spherical flower was constructed as a result of the stacking of leaf-shaped nanoflakes as building blocks. The TEM images (Fig. 6b and 6c) further demonstrated that catalyst **3** had worm-like mesostructural nanoflakes with a thickness of about 25 nm on the mesoporous ridge. It was worth mentioning that the TEM image with a chemical mapping technique (Fig. 6d) displayed the uniform distribution of the Rh centers within the silicate network, which would play an important role in dominating its catalytic performance, as discussed below. Based on the above studies, a safe conclusion could be drawn, in which $Cp^*RhTsDPEN$ -functionalized mesoporous silica with a uniform distribution of Rh centers could be readily obtained in this case.

Catalytic properties of the heterogeneous catalyst

As a type of highly active catalyst, homogeneous $Cp^*RhTsDPEN$ catalysts are used extensively in the asymmetric transfer hydrogenation of ketones in aqueous media.^{9,10} Due to its typical two-phase catalysis system in the asymmetric reaction, it often needs Bu_4NBr to act as a phase transfer catalyst to enhance its catalytic efficiency. In this case, because of the

salient phase transfer feature of the residual CTAB functionality, this asymmetric transfer hydrogenation catalyzed by catalyst **3** was carried out in the absence of a Bu_4NBr system, in which HCO_2Na worked as a hydrogen source and 1.0% mol of FFMS silica acted as a catalyst, according to the reported methods.^{10a} Taking acetophenone as an example, catalyst **3** gave (*S*)-1-phenyl-1-ethanol with more than 99% conversion and 97% ee, in which the conversion was obviously higher than that of its homogeneous counterpart (Table 1, entry 1 *versus* entry 1 in bracket) while the ee value was comparable to that of its homogeneous counterpart and even to that of its homogeneous counterpart with Bu_4NBr as a phase transfer catalyst.^{10a} In addition, this asymmetric reaction of acetophenone could also be completed with the same result on a large scale using 10.0 mmol of acetophenone as the substrate. Of particular note, was that the reaction could be run at a high ratio of substrate to catalyst without affecting its ee value, as exemplified by the asymmetric transfer hydrogenation of acetophenone with a substrate/catalyst ratio = 500 (Table 1, entry 2).

Based on the above excellent catalytic efficiency, catalyst **3** was investigated systematically in the asymmetric transfer hydrogenation of various substrates in the absence of Bu_4NBr . As shown in Table 1, excellent conversions, no side products, and high enantioselectivities were obtained under similar conditions. It was worth mentioning that the asymmetric reactions for all tested substrates could be completed within a short reaction time relative to those of its counterpart in the

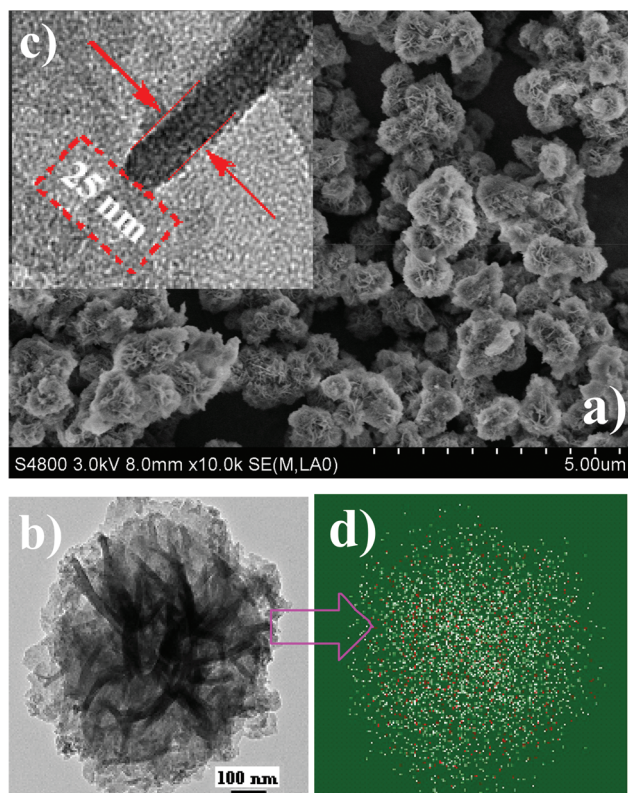


Fig. 6 (a) The SEM image of **3**, (b) the TEM image of **3**, (c) the TEM image of the mesoporous ridges and (d) a chemical mapping of **3** showing the distribution of Si (white) and Rh (red).

Table 1 Asymmetric transfer hydrogenation of aromatic ketones^a

Entry	Ar	Time [h]	Conv. ^b [%]	ee ^b [%]
1	Ph	0.5	>99 (88)	97 ^c (96)
2	Ph	4.0	86	97 ^d
3	Ph	0.5	97	95 ^e
4	Ph	0.5	>99	96 ^f
5	4-FPh	0.5	>99	92
6	4-ClPh	0.5	>99	94
7	4-BrPh	0.5	>99	94
8	3-BrPh	0.5	>99	97
9	4-MePh	2.0	>99	94
10	4-OMePh	4.0	97	94
11	3-OMePh	0.5	>99	95
12	4-CNPh	0.5	>99	89
13	4-CF ₃ Ph	0.5	>99	94
14	4-NO ₂ Ph	0.5	>99	86
15	1-Pyrenyl	24.0	46 (79)	55 ^c (81)

^a Reaction conditions: catalyst (7.58 mg, 2.00 μmol of Rh based on ICP analysis), HCO_2Na (0.68 g, 10.0 mmol), ketone (0.20 mmol) and 2.0 mL water, reaction temperature (313 K), reaction time (0.5–5.0 h).

^b Determined by chiral GC or HPLC analysis (see ESI in Fig. S4†). ^c Data were obtained using the homogeneous $Cp^*RhTsDPEN$ catalyst without the addition of Bu_4NBr in aqueous medium. ^d Data was obtained with 0.2% mol of catalyst. ^e Data were obtained using $TsDPEN$ -functionalized-FFMS (**2**) plus $(Cp^*RhCl_2)_2$ as a catalyst. ^f Data were obtained using the pure FMS material plus $Cp^*RhTsDPEN$ as a catalyst.

Table 2 Reusability of catalyst **3** for the asymmetric transfer hydrogenation of acetophenone^{a,b}

Run time	1	2	3	4	5	6	7	8	9	10
Conv. [%]	99.9	99.9	99.9	99.9	99.9	99.9	99.7	99.6	99.1	98.3
ee [%]	97.5	97.5	97.5	97.4	97.4	97.0	97.4	97.2	97.0	96.0

^a Reaction conditions: catalyst (7.58 mg, 2.00 μ mol of Rh based on ICP analysis), HCO₂Na (0.68 g, 10.0 mmol), ketone (0.20 mmol) and 2.0 mL water, reaction temperature (313 K), reaction time (0.5–4.0 h). ^b Determined by chiral GC analysis (see ESI in Fig. S5†).

absence of Bu₄NBr, demonstrating its bifunctionalized feature. Notably, the superior catalytic activity could be attributed to the salient phase-transfer functions of the residual CTAB functionality in a two-phase catalysis system. The comparable enantioselectivity should be due to the fact that the active rhodium center within its FFMS silicate network could maintain its original chiral microenvironment, as verified by XPS spectra in Fig. 4.

To gain better insight into the nature of the heterogeneous catalysis and to eliminate non-covalent adsorption during the catalytic process, two parallel experiments were carried out using TsDPEN-functionalized-FFMS (**2**) plus (Cp*RhCl₂)₂ and the pure FFMS material plus homogeneous Cp*RhTsDPEN as the heterogeneous catalysts. It was found that the asymmetric reaction in the former afforded the corresponding alcohol with 97% conversion and 95% (Table 1, entry 3), while that in the latter gave the alcohol with more than 99% conversion and 96% ee (Table 1, entry 4). The former suggested that the catalyst synthesized by the *in situ* complexation method could result in a catalytic performance. The slightly lower catalytic activity and enantioselectivity than those observed for catalyst **3** could be ascribed to the fact that the small parts of (Cp*RhCl₂)₂ were not coordinated during the catalytic process. The loss of Rh could be detected by ICP analysis in solution. The comparable conversion and enantioselectivity in the latter case indicated that the homogeneous catalyst, *via* the non-covalent physical adsorption, retained its original catalytic efficiency. However, when this catalyst in the latter case was underwent a process of Soxhlet extraction, the reused catalyst gave only a small products. This fact ruled out the role of the non-covalent physical adsorption, demonstrating that the nature of the heterogeneous catalysis was indeed derived from the heterogeneous catalyst itself.

Also, it was noted that catalyst **3** exhibited size selectivity toward some substrates. Due to the size constraint and reduced accessibility of the activation sites, a large size 1-acetylpyrene (Table 1, entry 15), was difficult to be transformed completely even after a prolonged reaction time, in which only 46% conversion and 55% ee was observed within 24 hours. To further confirm the size selectivity, a comparable experiment was investigated, in which the reaction of a mixture of catalyst **3** and two equivalent mole reactants (small acetophenone and large 1-acetylpyrene) was carried out under similar conditions. It was found that acetophenone could be transformed quantitatively, while only 8% conversion of 1-acetylpyrene was obtained within 0.5 hour, confirming the presence of the size selectivity.

Important features to include in the design of any heterogeneous catalyst is easy separation *via* simple filtration, and the retention of catalytic activity and enantioselectivity in the recovered catalyst after multiple cycles. As shown in Table 2, the heterogeneous catalyst **3** was recovered easily and reused repeatedly when acetophenone was chosen as the substrate. Remarkably, in ten consecutive reactions, the recycled catalyst **3** still afforded (*S*)-1-phenyl-1-ethanol with 98% conversion and 96% ee. The high recyclability could be due to the fact that the highly dispersed Cp*RhTsDPEN active centers *via* strong covalent-bonding immobilization within the FFMS network, as verified by the TEM chemical mapping, can efficiently decrease the leaching of Rh. Evidence to support this reasoning came from the ICP analysis, in which the amount of Rh after the tenth recycle was 26.16 mg per gram catalyst and only 4.8% of Rh was lost, demonstrating that the high recyclability could be due to the low leaching of Rh.

Conclusions

In conclusion, we have developed organorhodium-functionalized flower-like mesoporous silica, which was constructed by ultrathin perpendicularly aligned mesoporous nanoflakes *via* a cooperative dual-template approach. The developed bifunctionalized heterogeneous catalyst, exhibits excellent catalytic activity and high enantioselectivity in the asymmetric transfer hydrogenation of aromatic ketones in aqueous medium. More importantly, the residual surfactant within its mesoporous silicate network acted as a phase transfer catalyst that could enhance greatly the catalytic activity, while the confined chiral organorhodium complex bonded within its mesoporous silicate network could maintain a similar enantioselectivity to its homogeneous counterpart. Furthermore, this heterogeneous catalyst could be recovered easily and reused repeatedly ten times without any obvious affects on its catalytic performance, showing a good potential for use in industrial applications. In particular, this immobilized strategy does not only highlight a new way to immobilize various chiral homogeneous catalysts but also promotes the catalytic efficiency *via* a synergistic effect of the salient phase-transfer function and the catalytic nature of the confined chiral organorhodium.

Acknowledgements

We are grateful to the China National Natural Science Foundation (20673072), the Shanghai Sciences and Technologies Development Fund (10DJ1400103, 10JC1412300 and

12nm500500), the CSIRT (IRT1269) and the Shanghai Municipal Education Commission (12ZZ135) for financial support.

References

- (a) P. J. Walsh, H. M. Li and C. A. de Parrodi, *Chem. Rev.*, 2007, **107**, 2503; (b) C. E. Song, in *Handbook of Asymmetric Heterogeneous Catalysis*, ed. K. L. Ding and Y. Uozumi, Wiley-VCH, Weinheim, 2009, p. 25; (c) J. M. Thomas and R. Raja, *Acc. Chem. Res.*, 2008, **41**, 708; (d) M. Heitbaum, F. Glorius and I. Escher, *Angew. Chem., Int. Ed.*, 2006, **45**, 4732; (e) C. Li, H. D. Zhang, D. M. Jiang and Q. H. Yang, *Chem. Commun.*, 2007, 547; (f) M. Bartók, *Chem. Rev.*, 2010, **110**, 1663.
- (a) J. M. Thomas and R. Raja, *Acc. Chem. Res.*, 2008, **41**, 708; (b) R. Raja, J. M. Thomas, M. D. Jones, B. F. G. Johnson and D. E. W. Vaughan, *J. Am. Chem. Soc.*, 2003, **125**, 14982.
- (a) D. M. Jiang, J. S. Gao, Q. H. Yang, J. Yang and C. Li, *Chem. Mater.*, 2006, **18**, 6012; (b) P. N. Liu, P. M. Gu, F. Wang and Y. Q. Tu, *Org. Lett.*, 2004, **6**, 169; (c) D. M. Jiang, Q. H. Yang, J. Yang, L. Zhang, G. R. Zhu, W. G. Su and C. Li, *Chem. Mater.*, 2005, **17**, 6154.
- (a) H. Q. Yang, L. Zhang, L. Zhong, Q. H. Yang and C. Li, *Angew. Chem., Int. Ed.*, 2007, **46**, 6861; (b) H. Q. Yang, J. Li, J. Yang, Z. M. Liu, Q. H. Yang and C. Li, *Chem. Commun.*, 2007, 1086.
- (a) A. Thomas, *Angew. Chem., Int. Ed.*, 2010, **49**, 8328; (b) N. Mizoshita, T. Taniab and S. Inagaki, *Chem. Soc. Rev.*, 2011, **40**, 789; (c) F. Hoffmann and M. Fröba, *Chem. Soc. Rev.*, 2011, **40**, 608.
- (a) S. Y. Bai, H. Q. Yang, P. Wang, J. S. Gao, B. Li, Q. H. Yang and C. Li, *Chem. Commun.*, 2010, **46**, 8145; (b) H. Q. Yang, L. Zhang, P. Wang, Q. H. Yang and C. Li, *Green Chem.*, 2009, **11**, 257; (c) P. Y. Wang, X. Liu, J. Yang, Y. Yang, L. Zhang, Q. H. Yang and C. Li, *J. Mater. Chem.*, 2009, **19**, 8009.
- (a) M. E. Davis, *Nature*, 2002, **417**, 813; (b) L. Zhang, S. Z. Qiao, Y. G. Jin, H. G. Yang, S. Budihartono, F. Stahr, Z. F. Yan, X. L. Wang, Z. P. Hao and G. Q. Lu, *Adv. Funct. Mater.*, 2008, **18**, 3203; (c) H. Zhang, Z. Li, P. Xu, R. Wu and Z. Jiao, *Chem. Commun.*, 2010, **46**, 6783.
- L. Zhang, Y. N. Guo, J. Peng, X. Liu, P. Yuan, Q. H. Yang and C. Li, *Chem. Commun.*, 2011, **47**, 4087.
- (a) T. Ikariya and A. J. Blacker, *Acc. Chem. Res.*, 2007, **40**, 1300; (b) J. E. D. Martins, G. J. Clarkson and M. Wills, *Org. Lett.*, 2009, **11**, 847; (c) R. Malacea, R. Poli and E. Manoury, *Coord. Chem. Rev.*, 2010, **254**, 729.
- (a) X. F. Wu, X. H. Li, A. Zanotti-Gerosa, A. Pettman, J. Liu, A. J. Mills and J. L. Xiao, *Chem.-Eur. J.*, 2008, **14**, 2209; (b) X. F. Wu, J. Liu, D. D. Tommaso, J. A. Iggo, C. R. Catlow, J. Bacsá and J. L. Xiao, *Chem.-Eur. J.*, 2008, **14**, 7699; (c) P. N. Liu, J. G. Deng, Y. Q. Tu and S. H. Wang, *Chem. Commun.*, 2004, 2070; (d) N. A. Cortez, G. Aguirre, M. Parra-Hake and R. Somanathan, *Tetrahedron Lett.*, 2009, **50**, 2228.
- (a) Y. Q. Sun, G. H. Liu, H. Y. Gu, T. Z. Huang, Y. L. Zhang and H. X. Li, *Chem. Commun.*, 2011, **47**, 2583; (b) G. H. Liu, J. Y. Wang, T. Z. Huang, X. H. Liang, Y. L. Zhang and H. X. Li, *J. Mater. Chem.*, 2010, **20**, 1970; (c) G. H. Liu, M. Yao, F. Zhang, Y. Gao and H. X. Li, *Chem. Commun.*, 2008, 347; (d) W. Xiao, R. H. Jin, T. Y. Cheng, D. Q. Xia, H. Yao, F. Gao, B. X. Deng and G. H. Liu, *Chem. Commun.*, 2012, **48**, 11898; (e) J. Long, G. H. Liu, T. Y. Cheng, H. Yao, Q. Q. Qian, J. L. Zhuang, F. Gao and H. X. Li, *J. Catal.*, 2013, **298**, 41; (f) H. S. Zhang, R. H. Jin, H. Yao, S. Tang, J. L. Zhuang, G. H. Liu and H. X. Li, *Chem. Commun.*, 2012, **48**, 7874; (g) Y. L. Xu, J. Long, K. T. Liu, Q. Q. Qian, F. Gao, G. H. Liu and H. X. Li, *Adv. Synth. Catal.*, 2012, **354**, 3250.
- (a) G. H. Liu, Y. Q. Sun, J. Y. Wang, C. S. Sun, F. Zhang and H. X. Li, *Green Chem.*, 2009, **11**, 1477; (b) G. H. Liu, Y. Gao, X. Q. Lu, F. Zhang, M. M. Liu and H. X. Li, *Chem. Commun.*, 2008, 3184; (c) J. L. Huang, F. X. Zhu, W. H. He, F. Zhang, W. Wang and H. X. Li, *J. Am. Chem. Soc.*, 2010, **132**, 1492; (d) X. S. Yang, F. X. Zhu, J. L. Huang, F. Zhang and H. X. Li, *Chem. Mater.*, 2009, **21**, 4925; (e) K. T. Liu, R. H. Jin, T. Y. Cheng, X. M. Xu, F. Gao, G. H. Liu and H. X. Li, *Chem.-Eur. J.*, 2012, **18**, 15546.
- J. Mao and D. C. Baker, *Org. Lett.*, 1999, **1**, 841.
- P. F. W. Simon, R. Ulrich, H. W. Spiess and U. Wiesner, *Chem. Mater.*, 2001, **13**, 3464.
- T. Posset and J. Blumel, *J. Am. Chem. Soc.*, 2006, **128**, 8394.
- O. Krócher, O. A. Köppel, M. Fröba and A. Baiker, *J. Catal.*, 1998, **178**, 284.
- (a) H. X. Li, F. Zhang, Y. Wan and Y. F. Lu, *J. Phys. Chem. B*, 2006, **110**, 22942; (b) H. X. Li, Q. F. Zhao, Y. Wan, W. L. Dai and M. H. Qiao, *J. Catal.*, 2006, **244**, 251.
- V. Cauda, A. Schlossbauer, J. Kecht, A. Zürner and T. Bein, *J. Am. Chem. Soc.*, 2009, **131**, 11361.
- L. Wang, J. R. Sowa, C. Wang, R. S. Lu, P. G. Gassman and T. C. Flood, *Organometallics*, 1996, **15**, 4240.